JACS
JOURNAL OF THE AMERICAN CHEMICAL SOCIETY

Article

pubs.acs.org/JACS

Structure, Stability, and Properties of the Intergrowth Compounds $([SnSe]_{1+\delta})_m(NbSe_2)_n$, where $m = n = 1-20$

Matti B. Alemayehu,* Kim Ta, Matthias Falmbigl, and David C. Johnson*

Department of Chemistry and Materials Science Institute, University of Oregon, Eugene, Oregon 97403, United States

Supporting Information

ABSTRACT: Intergrowth compounds of $([SnSe]_{1+\delta})_m(NbSe_2)_n$, where $1 \leq m = n \leq 20$, with the same atomic composition but different *c*-axis lattice parameters and number of interfaces per volume were synthesized using the modulated elemental reactant technique. A *c*-axis lattice parameter change of 1.217(6) nm as a function of one unit of $m = n$ was observed. In-plane X-ray diffraction shows an increase in distortion of the rock salt layer as a function of *m* and a broadening of the $NbSe_2$ reflections as *n* increases, indicating the presence of different coordination environments for Nb (trigonal prismatic and octahedral) and smaller crystallite size, which were confirmed via scanning transmission electron microscopy investigations. The electrical resistivities of all 12 compounds exhibit metallic temperature dependence and are similar in magnitude as would be expected for isocompositional compounds. Carrier concentration and mobility of the compounds vary within a narrow range of $2-6 \times 10^{21}$ cm^{-3} and 2−6 $cm^2\ V^{-1}\ s^{-1}$, respectively. Even at a thickness of 12 nm for the SnSe and $NbSe_2$ blocks, the properties of the intergrowth compounds cannot be explained as composite behavior, due to significant charge transfer between them. Upon being annealed at 500 °C, the higher order $m = n$ compounds were found to convert to the thermodynamically stable phase, the (1,1) compound. This suggests that the capacitive energy of the interfaces stabilizes these intergrowth compounds.

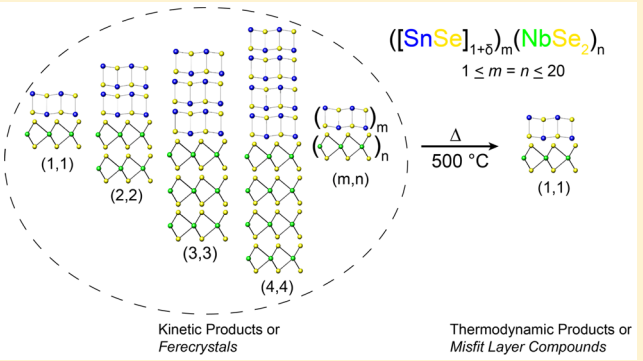

INTRODUCTION

The synthesis of solid phase materials has been dominated by traditional "heat and beat" methods in which solid reactants are mechanically mixed and heated at high temperatures to form desired compounds.[1−3] The high temperatures during synthesis are required to overcome slow diffusion rates in solids. Some of the disadvantages of these diffusion-limited reactions include incomplete reactions, compositionally inhomogeneous products, undesired nanostructures, and loss of control over the products, and typically only thermodynamically stable compounds form. An unusual example of thermodynamically stable compounds accessed through solid state synthesis are misfit layer compounds (MLCs).[4] MLCs have the generic formula $([MX]_{1+\delta})_m(TX_2)_n$, where M = Sn, Pb, Bi, Sb or rare earth metals, T = group IV or V transition metals, and X = S or Se. δ is the ratio of the in-plane areas of the two constituents, *m* is the number of MX layers, and *n* is the number of TX_2 slabs. Owing to their synthesis via high temperature sintering, MLCs only exist if they are thermodynamically stable, which limits them to the (1,1) and (1,2) compounds with few exceptions.[4] The reason for the formation of these intergrowth compounds rather than a mixture of the bulk solids has been the subject of significant debate.[4,5]

One way of overcoming the diffusion barrier in solid-state synthesis is through intimate mixing of reactants to minimize diffusion length (see Figure 1). The modulated elemental reactants technique (MER) is capable of fulfilling these prerequisites at an atomic scale and has demonstrated the ability to access specific metastable compounds.[6,7] In contrast to the misfit layer compounds, where a structural distortion of both constituents is required to accommodate one commensurate in-plane axis for both constituents,[4] while the other one remains incommensurate, via the MER technique a new subgroup of MLCs, so-called ferecrystals,[6−8] are formed, where the constituents exhibit rotational disorder and independent in-plane crystal structures resembling their bulk analogues. This lack of distortion together with the extensive rotational disorder between and even within the constituent units are the structural key features of ferecrystals. Furthermore, the MER technique allows access to compounds with specific *m* and *n*[9,10] as high as 20 and inorganic isomers,[11] which result from the precise control of the layering sequence to mimic the nanoarchitecture of the final product. Previously, reports on $([SnSe]_{1+\delta})_m(MoSe_2)_n$[9] demonstrated the ability to form high order compounds with $m = n$ up to 20. The ability to form the higher order compounds is somewhat surprising since the main stabilization mechanism for MLCs as well as ferecrystals is charge transfer between the constituents.[4,10,12] In the case of $m = n$ ferecrystalline compounds, where the thickness of the

Received: February 11, 2015
Published: March 25, 2015

DOI: 10.1021/jacs.5b01556
J. Am. Chem. Soc. 2015, 137, 4831−4839

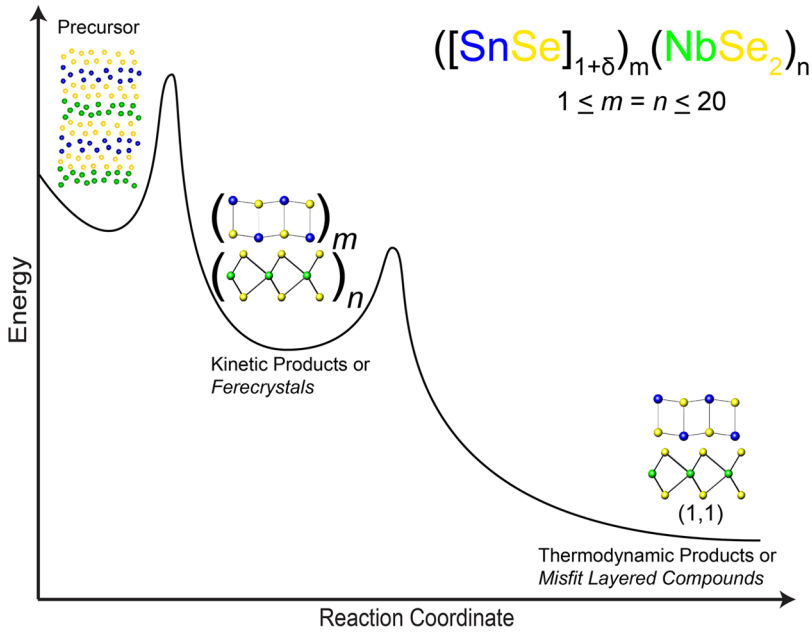

Figure 1. Schematic reaction pathway for the formation of ferecrystals and misfit layer compounds.

building blocks is increased while keeping the number of interfaces between the two constituents constant, a significant decline in the contribution of charge transfer stabilization is expected. In the case of $([SnSe]_{1+\delta})_m(MoSe_2)_n$[9] compounds, it was shown that the SnSe constituent exhibits a size-dependent *ab*-plane distortion toward its bulk analogue as $m = n$ is increased. This example clearly demonstrates that the volume free energy gains dominance over the surface free energy of the constituents as the thicknesses of the building blocks increase. This observation opens up the question if charge transfer stabilizes these higher order compounds or, if there is a crossover, where the intergrowth compounds turn into simple composite materials. The semiconducting $([SnSe]_{1+\delta})_m(MoSe_2)_n$[9] compounds do not allow a detailed investigation of this concept, as their electrical properties are dominated by the concentration of defects.[13]

The metallic compounds $([SnSe]_{1+\delta})_m(NbSe_2)_n$ with $m = n$ open an opportunity to answer this question, as the charge transfer behavior of these compounds was already extensively studied for different series of compounds such as $(m,1)$, $(m,2)$ and $(1,n)$.[10,14,15] In the $(m,1)$ compounds,[10] it was shown that charge transfer increases with increasing content of SnSe. This was also observed in a sequence of $(m, 2)$ compounds.[14] Increasing the thickness of the $NbSe_2$ layer while keeping the SnSe layer constant revealed that charge transfer follows the expected trend by continuously increasing carrier concentration.[15] Comparing the properties of the $m = n$ compounds to these results should determine what stabilizes these compounds and if charge transfer plays a role in the higher order compounds. Here, we report the synthesis and characterization of $([SnSe]_{1+\delta})_m(NbSe_2)_n$, where $1 \le m = n \le 20$, varying the thickness of the constituent layers from 0.6 to 12 nm, to determine if the compounds transform from an intergrowth into a composite material. At a length scale of 10 nm, in-plane X-ray diffraction, and STEM images indicate a bulk-like structure of the SnSe-layer. However, the intergrowth compounds still form. Resistivity remains constant as expected for isocompositional compounds with an almost constant carrier concentration. The carrier concentration of all compounds remains well below the value of what would be expected, if it behaved as a composite. This suggests the presence of significant charge transfer between the constituents even for these thicknesses. At a higher temperature, a transformation of the higher order $m = n$ compounds into the thermodynamically stable (1,1) compound was observed.

EXPERIMENTAL SECTION

$([SnSe]_{1+\delta})_m(NbSe_2)_n$ with $1 \le m = n \le 20$ compounds were synthesized using the MER technique as previously referenced.[16] Thermionic 3 kW electron beam guns (Sn and Nb) and a Knudson effusion cell (Se) were used to evaporate the metal sources onto (100) oriented Si substrates. Sn (99.99% purity), Nb (99.99% purity), and Se (99.99% purity) were evaporated at the rate of 0.04, 0.02, and 0.05 nm/s, respectively. INFICON Xtal quartz microbalance monitors placed 25 cm above each source were used to monitor the deposition rates. A LabVIEW program was used to position the substrates, which are mounted on a motorized stage, on top of each elemental source based on the preprogrammed sequential deposition scheme. Pneumatic shutters were used to control the amount of material deposited. The samples were annealed under inert conditions in a N_2 glovebox with O_2 < 0.6 ppm on a hot plate. Total film thickness and crystallinity of the compounds were determined by X-ray reflectivity (XRR) and X-ray diffraction (XRD), respectively.

Both X-ray techniques were performed on a Bruker AXS D8 diffractometer equipped with Göbel mirror and Bragg−Brentano optics geometry and a Cu Kα (0.154 nm) radiation source operated at 40 kV and 40 mA. In-plane X-ray diffraction data were obtained from the Advanced Photon Source (APS) at the Argonne National Lab, Beamline-33-C with an incident X-ray wavelength of 0.12652 nm for compounds with $m = n < 9$. The in-plane X-ray diffraction for the sample with $m = n = 20$ was conducted on a Rigaku SmartLab equipped with Cu Kα (0.154 nm) radiation. The peak positions and the full width at half maximum (fwhm) were extracted from least-squares fits using a standard peak shape function. The lattice parameters were determined using Bragg's law.

Atomic compositions of the films were determined on a Cameca SX-100. The procedures and analysis technique were previously described by Donovan et al.[17]

Cross- section samples for high-angle annular dark-field scanning transmission electron microscopy (HAADF-STEM) were prepared and thinned using the FEI Helios Nanolab 600 Dual Beam focused ion

DOI: 10.1021/jacs.5b01556
J. Am. Chem. Soc. 2015, 137, 4831−4839

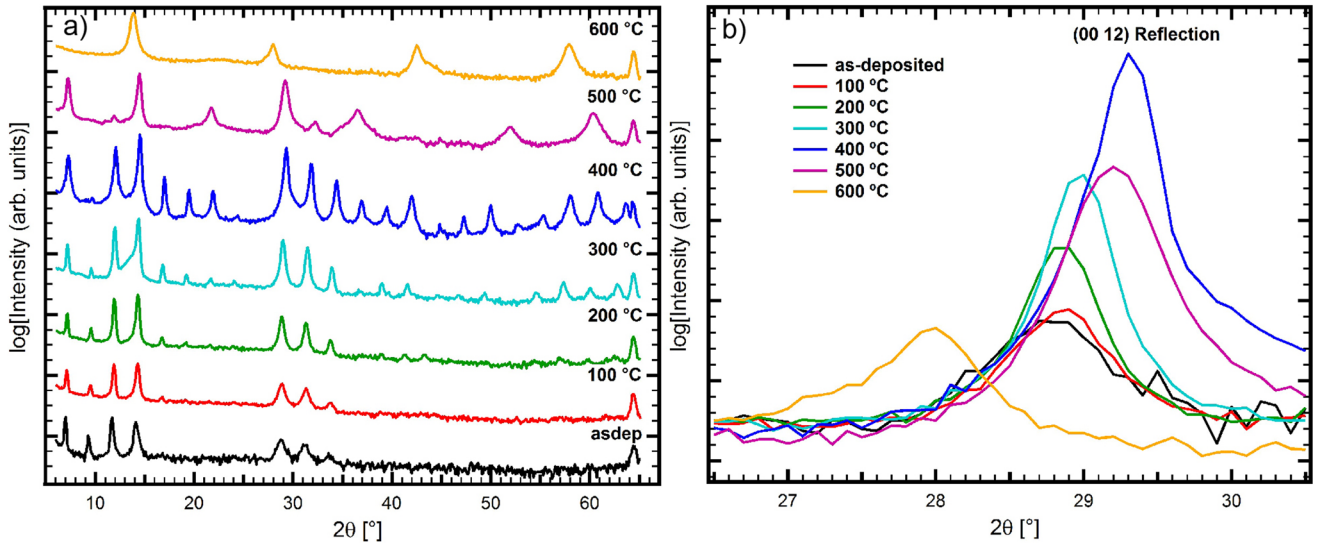

Figure 2. (a) Specular 00*l* X-ray diffraction patterns of the $([SnSe]_{1+\delta})_3(NbSe_2)_3$ compound after each annealing temperature for 20 min; (b) fwhm of the (00 12) reflection at different annealing temperatures with the sharpest and most intense reflection observed at 400 °C for 20 min.

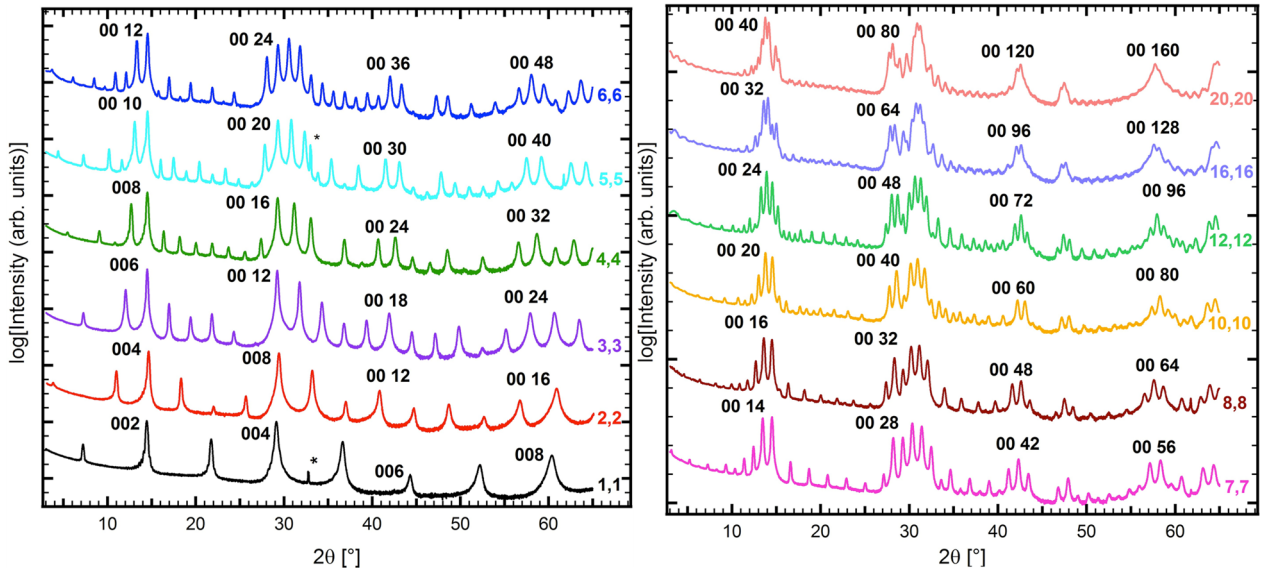

Figure 3. Specular 00*l* X-ray diffraction patterns of $([SnSe]_{1+\delta})_m(NbSe_2)_m$, for all 12 compounds, with selected Bragg reflections indexed to their corresponding *c*-lattice parameter. The asterisks (∗) mark silicon substrate peaks.

beam (FIB). These specimens were used for HAADF-STEM imaging on an FEI Titan 80-300.

Samples for electrical measurements were deposited onto fused quartz silica in a van der Pauw cross geometry. Four copper leads were contacted onto the four corners of the cross with indium. Current was then sourced through two of the cross arms and the potential between the remaining arms was measured using a nanovoltmeter. From the slope of the linear regression line for the current versus potential plot, the sheet resistance of the film was determined. Using the total thickness of the film, the sheet resistance was then converted into electrical resistivity. The measurements were conducted within a temperature range of 25−295 K. Hall measurements were carried out in a similar manner by applying different magnetic fields between 0 and 1.6 T.

■ RESULTS AND DISCUSSION

Precursors were prepared using the modulated elemental reactants (MER) technique with similar local composition, layer thickness, and layer sequence to that of the targeted final product. The calibration of the deposition required three steps. First, the ratio of the elements in the binary Sn/Se and Nb/Se layers were calibrated by keeping the amount of one elemental constituent constant in each bilayer and varying the other. The thickness and atomic composition of these compounds were determined via X-ray diffraction and EPMA and the ratio of deposition rates chosen to match the 1:1 and 1:2 stoichiometries of the constituents. Next, the ratio of Sn and Nb was adjusted to match the misfit ratio. Although, the misfit parameter changes as the thickness of the SnSe constituent increases, this change is too small to be compensated for with deposition times. Finally, the Sn:Se and Nb:Se bilayers were adjusted to the correct absolute thickness to yield one unit of SnSe and one unit of $NbSe_2$ respectively. The total thickness of the films was typically kept to 50 nm. After the precursors were prepared via physical vapor deposition, the self-assembly conditions were established by conducting an annealing study, which was performed on six pieces of the same

DOI: 10.1021/jacs.5b01556
J. Am. Chem. Soc. 2015, 137, 4831−4839

$([SnSe]_{1+\delta})_3(NbSe_2)_3$ precursor, for temperatures ranging between 100 and 600 °C for 20 min.

Optimal annealing time and temperature were determined by comparing the full width at half-maximum (fwhm) and intensity of the X-ray diffraction peaks of the annealed samples. Figure 2a shows the X-ray diffraction patterns of the annealing study. The continuous shift of the Bragg reflections to higher angles is indicative of loss of selenium (4−5 atom %) and shrinkage of the unit cell as a function of temperature (see Figure 2b). The sharpest and most intense 00*l* reflections are indicative of the highest degree of crystallographic alignment of the compound perpendicular to the substrate and the highest amount of the crystalline product. Figure 2b shows the fwhm of the (00 12) reflection at all annealing temperatures indicating that the optimal annealing condition is 400 °C for 20 min. One interesting phenomenon observed at 500 °C is the partial conversion of the (3,3) compound into a (1,1), which will be discussed in detail later in this paper.

Figure 3 shows the XRD patterns of the $([SnSe]_{1+\delta})_m(NbSe_2)_n$ compounds annealed at 400 °C, where $1 \leq m = n \leq 20$. All 00*l* reflections can be indexed to the corresponding *c*-axis lattice parameter and confirm the formation of highly oriented superlattices. By plotting the *c*-axis lattice parameters (see Table 1), as a function of *m* and *n*, the repeat thickness of one unit of $([SnSe]_{1+\delta})_m(NbSe_2)_n$ can be extracted from the slope of the linear regression line. The *c*-axis lattice parameter was determined to be 1.217(6) nm, which is slightly smaller than the *c*-axis lattice parameter of the (1,1) compound (1.225(2) nm).[18] This difference results from the different interfaces, which are added to the superlattice by increasing $m = n$ by 1. In contrast to the (1,1) compound, where the *c*-axis lattice parameter includes the distance between a SnSe and a $NbSe_2$ unit, here by increasing $m = n$ by one, half of a SnSe−SnSe distance and half of the van der Waals gap between consecutive $NbSe_2$ layers are added; hence, the smaller value of 1.217(6) nm originates from the comparably smaller SnSe−SnSe distances. The X-ray diffraction patterns together with atomic composition of each sample (listed in Table 1) confirm the formation of the isocompositional compounds with increasing thickness of the constituent layers.

Table 1. *c*-Axis Lattice Parameter, Atomic Composition and fwhm of $([SnSe]_{1+\delta})_m(NbSe_2)_n$ for the Reflection at 14° 2θ (00m + n)

$m = n$	*c*-axis lattice parameter [nm]	fwhm [deg]	atom % Sn	atom % Nb	atom % Se
1	1.225(2)	0.301(1)	20.6(5)	16.5(5)	57.2(5)
2	2.435(5)	0.265(1)	21.0(5)	16.8(5)	58.0(5)
3	3.654(9)	0.216(1)	21.8(5)	17.1(5)	57.8(5)
4	4.770(2)	0.257(1)	21.6(5)	17.6(5)	57.9(5)
5	6.070(1)	0.227(1)	21.2(5)	16.8(5)	57.4(5)
6	7.302(8)	0.222(1)	21.2(5)	17.4(5)	56.9(5)
7	8.535(8)	0.228(1)	20.4(5)	17.1(5)	57.8(5)
8	9.770(2)	0.235(1)	20.9(5)	17.0(5)	56.8(5)
10	12.10(8)	0.222(1)	21.5(5)	17.9(5)	57.0(5)
12	14.53(2)	0.210(1)	21.9(5)	17.2(5)	58.2(5)
16	19.40(1)	0.233(1)			
20	24.40(1)	0.230(1)	21.2(5)	17.5(5)	57.0(5)

In-plane X-ray diffraction patterns of the compounds displayed in Figure 4a reveal the presence of independent crystal structures for the two subunits, as reported previously for the (1,1) compound.[18] A prominent peak splitting of the SnSe reflections as a function of increasing *m* is observed. This indicates that the basal plane of the rock salt-like layer is distorted from square to a rectangle as reported previously for the series $([SnSe]_{1+\delta})_m(MoSe_2)_n$, $([SnSe]_{1+\delta})_m(NbSe_2)_1$, and $([SnSe]_{1+\delta})_m(NbSe_2)_2$.[10,14,19] The amount of distortion is independent of the $NbSe_2$-layer thickness indicating that the structural interaction between layers is minimal, which is in agreement with previous theoretical calculations.[19] The *ab*-plane distortion of the SnSe in the (20,20) compound from a square is 4% less than that found for the equilibrium bulk structure of orthorhombic SnSe at 300 K.[20] The *a* and *b* lattice parameters observed are exactly the same as that reported for a (20,2) compound (see Figure 4b).[14] This change in in-plane symmetry from a square to a rectangle mirrors as a function of size the second order phase transition reported for bulk-SnSe as a function of decreasing temperature.[20] The evolution of the in-plane lattice parameters with size suggests a competition between surface and volume free energy, with the volume free energy dominant at larger SnSe thickness compared to surface free energy.[19] The trend in in-plane lattice parameters indicates a transition from a thin bilayer of SnSe in an intergrowth compound dominated by surface free energy to a bulk-like

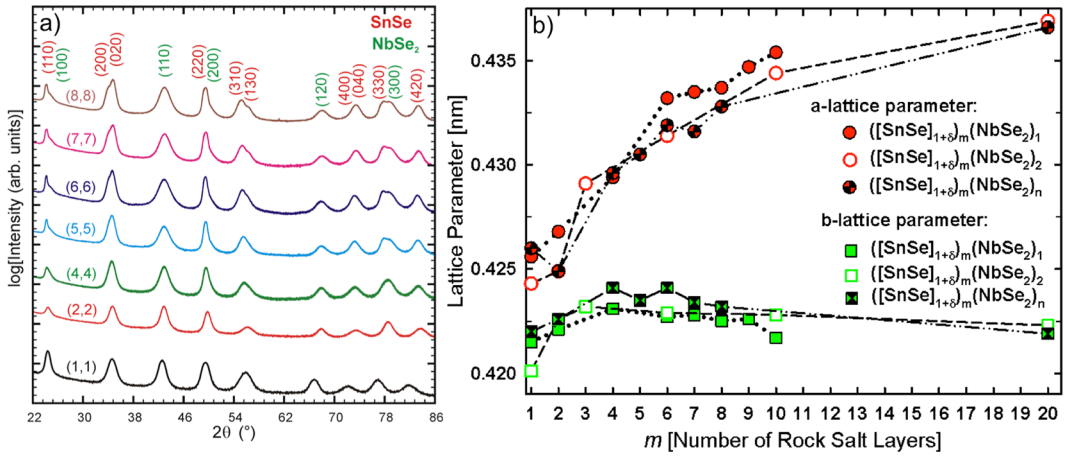

Figure 4. (a) In-plane X-ray diffraction patterns of $([SnSe]_{1+\delta})_m(NbSe_2)_n$ with $m = n$ 1−8. The Bragg-indices for the individual crystal structures are provided. (b) A comparison of the in-plane distortion in the SnSe constituent as a function of layer thickness for different series of $([SnSe]_{1+\delta})_m(NbSe_2)_n$: (*m*,1), (*m*,2), and ($m = n$).

DOI: 10.1021/jacs.5b01556
J. Am. Chem. Soc. 2015, 137, 4831−4839

Table 2. In-Plane Lattice Parameters of the SnSe and $NbSe_2$ Constituents, and the Resulting Misfit Parameter, δ, for $[(SnSe)_{1+\delta}]_m(NbSe_2)_n$ with $m = n$

	(1,1)	(2,2)	(4,4)	(5,5)	(6,6)	(7,7)	(8,8)	(20,20)
a-lattice SnSe (nm)	0.422(2)	0.4249(5)	0.4296(2)	0.4305(2)	0.4319(3)	0.4316(2)	0.4328(3)	0.4366(3)
b-lattice SnSe (nm)	0.426 (2)	0.4226(4)	0.4241(1)	0.4235(4)	0.4241(4)	0.4234(1)	0.4232(2)	0.4219(2)
a-lattice $NbSe_2$ (nm)	0.3459(2)	0.3463(1)	0.3462(1)	0.3459(1)	0.3458(1)	0.3453(2)	0.3454(1)	0.3456(1)
δ	0.152	0.156	0.139	0.135	0.137	0.130	0.128	0.110

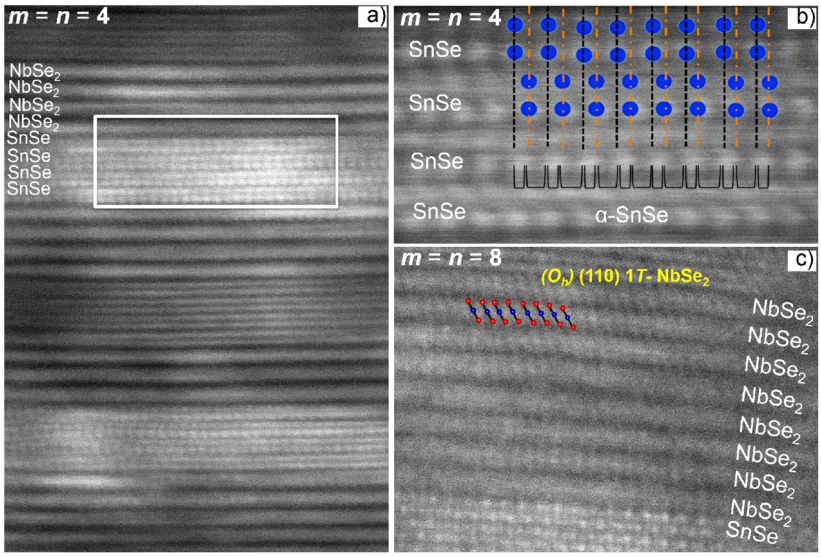

Figure 5. HAADF-STEM image of a (4,4) (a), highlighting the tetragonal phase of SnSe (b), with the octahedral coordination of $NbSe_2$ in an (8,8) compound (c).

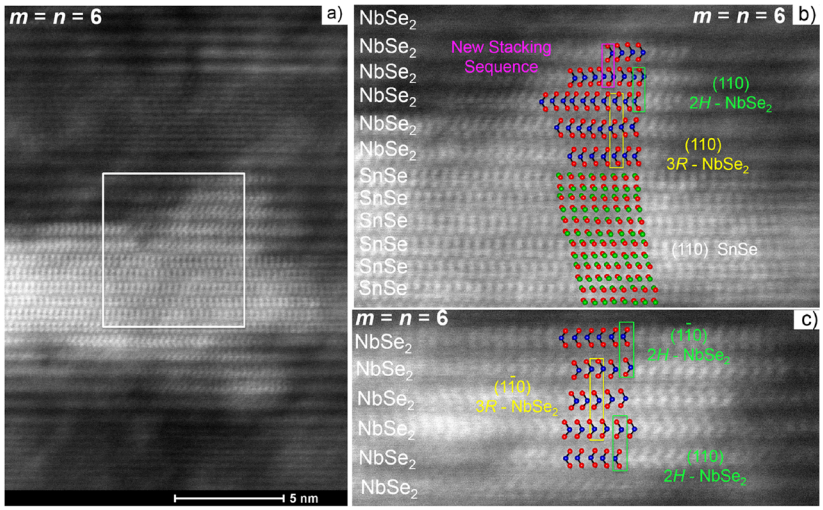

Figure 6. (a) HAADF-STEM image of a (6,6) compound with different stacking sequences of the $NbSe_2$ layers (b,c).

block as its thickness increases. Since the basal plane area increases in the SnSe as a function of *m* while the in-plane area of the $NbSe_2$ constituent remains constant, there is a corresponding decrease in the misfit ratio from 1.15 to 1.10. At higher *n*, a broadening of the $NbSe_2$ peaks is observed, suggesting shorter coherence lengths due to smaller grain sizes or a distribution of different coordination environments or stacking sequences, which result in different *a*-axis lattice parameters for different bulk polytypes.[21] STEM investigations, discussed later, show two distinct coordination environments for the Nb atoms, trigonal prismatic and octahedral, as well as different stacking sequences (see Figure 6). The *a*-axis lattice parameters range between 0.3454(1) nm and 0.3463(1) nm, which is slightly larger than the 2*H*-$NbSe_2$ (0.3449−0.3460(1) nm)[21,22] and smaller than the 1*T*-$NbSe_2$ ((0.353(1) nm)[21] in-plane lattice parameters (See Table 2).

Figure 5 displays representative HAADF-STEM images of a (4,4), and an (8,8) compound, which show abrupt atomic interfaces and rotational disorder between subsequent constituent layers. Generally, the intended stacking sequences were observed, for example, four trilayers of $NbSe_2$ followed by four double layers of SnSe in the (4,4) compound (see Figure 5a,b). A closer inspection revealed that on the basis of the spacing between consecutive SnSe bilayers, the SnSe constituent in the

DOI: 10.1021/jacs.5b01556
J. Am. Chem. Soc. 2015, 137, 4831−4839

(4,4) compound can unambiguously be classified as α-SnSe (see Figure 5b), which is consistent with the rectangular basal plane observed in the in-plane diffraction pattern.[23] Figure 5c depicts an area of an (8,8) compound where instead of the typical chevron observed for the (110) zone axis with trigonal prismatic coordination for Nb, we observe a linear arrangement which is diagnostic for octahedral coordination.[22] This might be due to charge transfer from the SnSe layer, which affects the electronic structure of the $NbSe_2$, or the probable nucleation of this coordination during self-assembly. A similar change in coordination environment was previously reported for (m,1) compounds as well as Li intercalated MoS_2.[10,24]

With increasing thickness of $NbSe_2$, the chance of crystallizing more diverse stacking sequences is possible.[15] Figure 6a displays an HAADF-STEM image of a (6,6) compound where six double layers of SnSe alternate with six trilayers of $NbSe_2$. Close scrutiny reveals different stacking sequences for the dichalcogenide constituent. Figure 6b,c show examples of six consecutive $NbSe_2$ layers, which crystallize in multiple stacking sequences and can be identified as fragments of the well-established polytypes for bulk $NbSe_2$[22] as well as novel sequences. The presence of rotational disorder and variety of stacking sequences clearly demonstrate that these compounds are kinetically trapped rather than thermodynamically stable and support the templating in random orientations of one layer to the next, as suggested by Atkins et al.[8] No correlation between the thickness of the $NbSe_2$ constituent (n) and the occurrence of a specific polytype was found.[15]

Our annealing study of the first eight compounds ($m = n$ (1−8)) showed that annealing at 500 °C for 20 min caused all of the compounds to start converting into their thermodynamically stable phase, namely the (1,1) compound: $([SnSe]_{1+\delta})_1(NbSe_2)_1$. This observation was corroborated by X-ray diffraction, X-ray reflectivity, and HAADF-STEM data. In the 00l diffraction scans displayed in Figure 7, superlattice peaks corresponding to a (1,1) repeat structure can be indexed after annealing a (3,3) sample at 500 °C, and only a few weak reflections remain that can be indexed to the (3,3) compound. The relative intensities of the Bragg reflections corresponding to the $([SnSe]_{1+\delta})_1(NbSe_2)_1$ compound in Figure 7 agree with that observed for the (1,1) compound (also displayed in Figure 7). X-ray reflectivity measurements taken during the annealing study of the (3,3) compound support its conversion into a (1,1) compound, as the (1,1) superlattice peak is still present at 500 °C while the (3,3) superlattice peaks decay almost completely. The Kiessig fringes arise from the constructive interference of the back and front of the film and can be used to calculate the total thickness of the film. After annealing at 500 °C, the film thickness is calculated to be 45.79(1) nm, 8.0 nm less than that of the sample annealed at 400 °C. This corresponds to a loss of approximately 2 unit cells of the initial (3,3) superlattice. There is also a loss of Kiessig fringes at angles >3° in 2θ after annealing at 500 °C, as a result of an increase in the roughness of the film due to the rearrangement of the layers and surface oxidation.

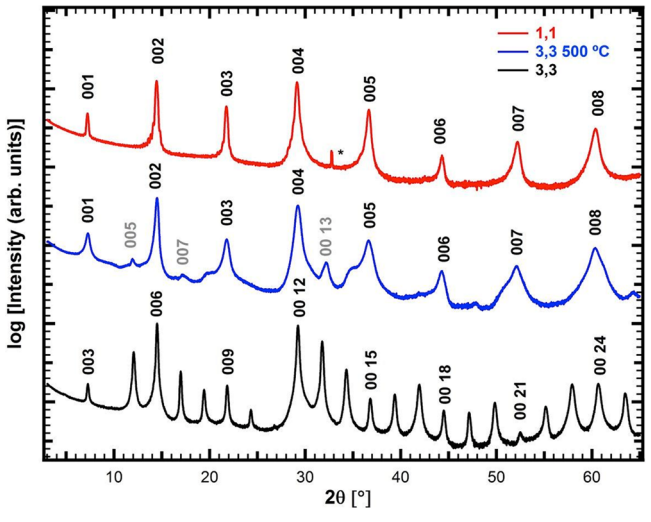

Figure 7. 00l X-ray diffraction patterns of the (3,3) compound at 500 °C (blue) showing the characteristic peaks of the thermodynamically stable compound: $([SnSe]_{1+\delta})_1(NbSe_2)_1$. The gray indices correspond to the remaining parent (3,3) compound and the black indices to the (1,1) superstructure (the corresponding diffraction patterns of the (3,3) and (1,1) compounds annealed at 400 °C are given for comparison in black and red, respectively). The asterisk (∗) marks Si-substrate peaks.

HAADF-STEM images of a region in the process of transforming from a (3,3) to a (1,1) compound is provided in Figure 8. A portion of the sample was observed to remain in the (3,3) superlattice, while the majority of the film was converted into a surprisingly homogeneous and smooth (1,1) stacking sequence. Figure 8a shows the unzipping of two $NbSe_2$ layers with SnSe to form the (1,1) compound revealing an interesting mechanism of the transformation. This is clearly illustrated in Figure 8b, which shows the formation of an intermediate SnSe layer within the van der Waals gap between two $NbSe_2$ layers. This observation clearly demonstrates the diffusion driven lowering of the total energy of the compound by generating a larger number of SnSe−$NbSe_2$ interfaces. The phenomenon of unzipping of dichalcogenide layers with an intercalant was previously reported in C_4−C_9 amine intercalated TaS_2 and is used to cleave the dichalcogenides into single sheets.[25] Figure 8c, clearly shows 18 consecutive layers of a (1,1) compound with a perfect layering sequence and atomically abrupt interfaces between the constituent layers.

This is the first report of which we are aware that shows a transformation of a high order superlattice into the thermodynamically stable product. It is well-known that the formation of misfit layer compounds using classic high-temperature synthesis techniques is limited to the thermodynamically stable product, usually a (1,1) compound. There are no reports on compounds with higher $m = n$ accessible by other techniques than the MER technique. Although the stability of these intergrowth compounds was debated for a long time, recent studies on (m,1) compounds of PbSe and SnSe unequivocally demonstrate the presence of significant charge transfer between the constituent layers.[10,12] In this case, the "capacitive" energy gain from this charge transfer is more favorable than the sum of the bonding energy between two SnSe layers and the weak van der Waals interaction between two dichalcogenide layers. This thermodynamically favors the formation of a (1,1) layering sequence.

Electrical Properties. Figure 9a shows the temperature-dependent resistivity of all 12 compounds. The magnitude of the resistivity of all samples is consistent with being metals, and they exhibit metallic temperature dependencies in the temperature range of 20−295 K. Prior studies of misfit layer compounds and ferecrystals indicate that the dichalcogenide constituent determines the conductivity behavior of these intergrowth compounds, presumably due to the higher carrier

DOI: 10.1021/jacs.5b01556
J. Am. Chem. Soc. 2015, 137, 4831−4839

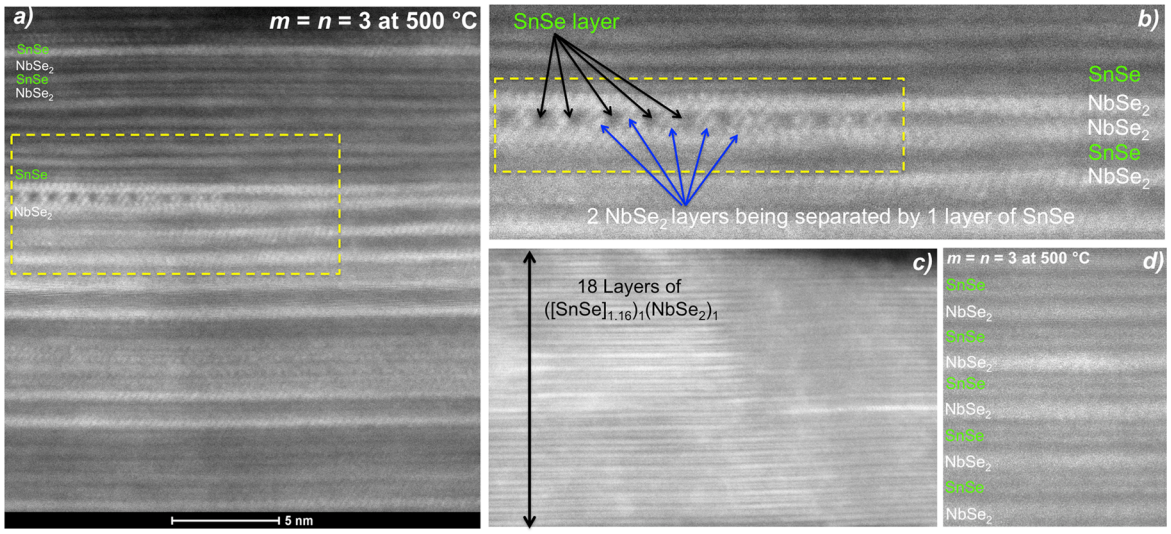

Figure 8. (a) The formation of a (1,1) superlattice from a (3,3) via separation of two $NbSe_2$ layers with one SnSe layer; (b) a zoom in image of the formation of the (1,1) compound; (c) the top to bottom view of the HAADF-STEM image showing 18 layers of a (1,1) compound; (d) the layering of a (1,1) is highlighted.

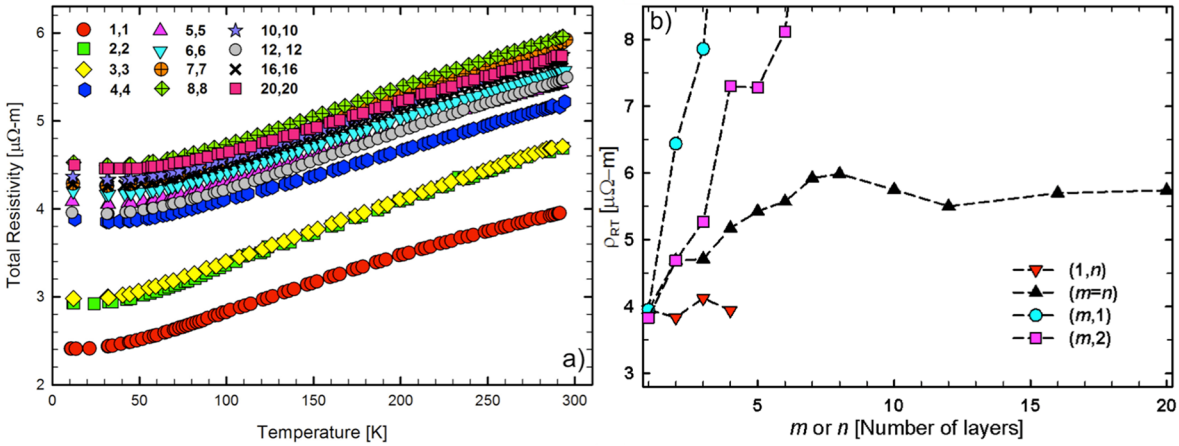

Figure 9. (a) Temperature-dependent resistivity of $([SnSe]_{1+\delta})_m(NbSe_2)_n$ where $m = n = 1-20$. (b) Comparison of room temperature resistivity as a function of layer thickness for $(m,1)$,[9] $(m,2)$,[14] $(1,n)$[15] and $(m = n)$ compounds.

concentration in the metallic dichalcogenide layers.[4,9−12] In general, the resistivity systematically increases with increasing $m = n$. For $m = n$ values between 1 and 4 the change in magnitude is comparably high, whereas compounds with $m = n$ values from 4−20 have almost the same magnitude and no trend in resistivity with m. In all cases the magnitude as well as the temperature dependence of the resistivity remains distinctly different from bulk $NbSe_2$ indicating the crossover to a composite behavior is not yet reached at $m = n = 20$. Compared to previously reported $(m,1)$, $(m,2)$, and $(1,n)$ compounds, the room temperature resistivities of the $(m = n)$ compounds are within a very narrow range of 4 to 6 $\mu\Omega$-m, while $(m,1)$ and $(m,2)$ spread over a wide range of 4−80 $\mu\Omega$-m and 4−52 $\mu\Omega$-m, respectively (see Figure 9b).[10,14] This wide range was reported to result from increasing charge transfer and an increase in the relative thickness of the less conductive SnSe constituent (4×10^4 to 1.8×10^6 $\mu\Omega$-m in bulk).[26]

To shed light onto what dominates the transport properties of the title compounds, Hall effect measurements were conducted. The carrier concentration and mobility were calculated applying the single band approximation for room temperature values, as displayed in Figure 10. The carrier concentration of an equivalent compound with composite behavior assuming bulk carrier concentrations for both constituents (SnSe and $NbSe_2$) weighed by their volume fraction is indicated by a dashed blue line (see Figure 10). The lower carrier concentration observed for all of the intergrowth compounds reveals the presence of a considerable amount of charge transfer. The initial systematic decrease in the carrier concentration for $m < 6$ suggests that the amount of charge donated per SnSe layer increases in this regime. The nearly linear increase in carrier concentration for $m > 6$ indicates a decrease in the amount of charge donated per SnSe layer and suggests that the charge depletion length is about this thickness and that the inner SnSe layers no longer donate much charge to the $NbSe_2$ layers. The in-plane structure of the SnSe changes as a function of m as well as the thickness of the layer, complicating a simple picture based on thickness alone. The transition that leads to a simple composite behavior with bulk structures and electrical properties that are a simple weighted sum of the bulk constituents is not yet reached for 20 repeat units of each constituent.

DOI: 10.1021/jacs.5b01556
J. Am. Chem. Soc. 2015, 137, 4831−4839

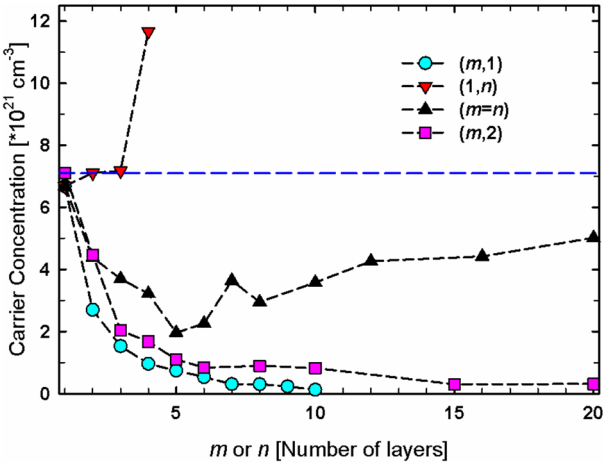

Figure 10. Room temperature carrier concentration of $(m,1)$, $(m,2)$, $(1,n)$, and $(m = n)$ with the carriers of $NbSe_2$ in half of the bulk $NbSe_2$ unit cell represented by a dashed blue line.

The mobility of the $m = n$ compounds varies only within a narrow range between 2 and 6 $cm^2\ V^{-1}\ s^{-1}$, which resides between the higher mobility of the $(m,1)$ and $(m,2)$ and the lower mobility of the $(1,n)$ compounds.[10,14,15] This could result from the competing effects of charge transfer, as in the case of the $(m,1)$ and $(m,2)$ compounds, and the higher degree of structural disorder arising from different stacking sequences as already observed for the $(1,n)$ compounds.[10,14,15] In general, these compounds with similar composition, but different amount and kind of interfaces per volume exhibit only subtle changes in electrical resistivity, carrier concentration, and mobility.

CONCLUSION

The synthesis of isocompositional ferecrystalline compounds $([SnSe]_{1+\delta})_m(NbSe_2)_n$, where $1 \leq m = n \leq 20$, with different c-axis lattice parameters and number of interfaces per unit volume is reported. The c-axis lattice parameter changes by 1.217(6) nm as one SnSe and $NbSe_2$ unit are added to the unit cell. In-plane diffraction shows independent crystal structures for both constituents, an increase in distortion of the SnSe layer as m increases becoming more similar to bulk-SnSe, and a broadening of the $NbSe_2$ peaks as a function of n indicating a smaller crystallite size and the presence of different coordination environments for the Nb atom: trigonal prismatic and octahedral. For the first time it was shown that the metastable higher order compounds convert into the thermodynamically stable (1,1) compound upon annealing at 500 °C. STEM images revealed rotational disorder and the conversion mechanism, where a SnSe layer diffuses into the van der Waals gap between two $NbSe_2$-layers, resulting in atomically abrupt interfaces of the (1,1) layering sequence. The electrical properties of these isocompositional compounds do not show a strong dependence on the change of interfaces per volume. The electrical resistivity, carrier concentration, and mobility remain constant and independent of the layer thickness. Only subtle changes at low $m = n$ values are observed and even at the largest thicknesses of the constituent layers no indication of a transition to a simple composite behavior was found. This demonstrates that charge transfer still plays a significant role in the higher order compounds.

ASSOCIATED CONTENT

Supporting Information

Schematic unit cell representation of the (2,2) and (4,4) compounds; specular X-ray diffraction patterns of $m = n \leq 8$ collected after an annealing at 500 °C for 20 min. This material is available free of charge via the Internet at http://pubs.acs.org.

AUTHOR INFORMATION

Corresponding Authors

davej@uoregon.edu
matti@uoregon.edu

Notes

The authors declare no competing financial interest.

ACKNOWLEDGMENTS

The authors thank R. Fischer and J. Razink from CAMCOR for assistance in preparing TEM samples and collecting STEM images. Grant MRI 0923577 provided funding for the dual beam FIB used to make TEM cross sections. The authors acknowledge support from the National Science Foundation under Grant DMR-1266217. Co-author MF acknowledges support from the National Science Foundation through CCI Grant No. CHE-1102637. The authors thank Jenia Karapetrova for assistance at Beamline 33-C at the Advanced Photon Source (APS) in Argonne National Laboratories. The use of the APS was supported by the U.S. Department of Energy, Office of Science, and the Office of Basic Energy Sciences, under Contract No. DE-AC02-06CH11357.

REFERENCES

(1) Rouxel, J.; Meerschaut, A.; Wiegers, G. A. *J. Alloys Compd.* **1995**, *229*, 144−157.
(2) Wiegers, G. A. *J. Alloys Compd.* **1995**, *219*, 152−156.
(3) Cario, L.; Palvadeau, P.; Lafond, A.; Deudon, C.; Moe, Y. *Chem. Mater.* **2003**, 943−950.
(4) Wiegers, G. A. *Prog. Solid State Chem.* **1996**, *24*, 1−139.
(5) Kalläne, M.; Rossnagel, K.; Marczynski-Bühlow, M.; Kipp, L.; Starnberg, H.; Stoltz, S. *Phys. Rev. Lett.* **2008**, *100*, 065502.
(6) Beekman, M.; Heideman, C. L.; Johnson, D. C. *Semicond. Sci. Technol.* **2014**, *29*, 064012.
(7) Moore, D. B.; Beekman, M.; Disch, S.; Johnson, D. C. *Angew. Chem., Int. Ed. Engl.* **2014**, *53*, 5672−5.
(8) Atkins, R.; Moore, D. B.; Johnson, D. C. *Chem. Mater.* **2013**, *25*, 1744−1750.
(9) Beekman, M.; Cogburn, G.; Heideman, C.; Rouvimov, S.; Zschack, P.; Neumann, W.; Johnson, D. C. *J. Electron. Mater.* **2012**, *41*, 1476−1480.
(10) Alemayehu, M. B.; Falmbigl, M.; Ta, K.; Grosse, C.; Westover, R. D.; Bauers, S. R.; Fischer, S. F.; Johnson, D. C. *Chem. Mater.* **2015**, *27*, 867−875.
(11) Esters, M.; Alemayehu, M. B.; Jones, Z.; Nguyen, N. T.; Anderson, M. D.; Grosse, C.; Fischer, S. F.; Johnson, D. C. *Angew. Chem., Int. Ed. Engl.* **2015**, *54*, 1130−1134.
(12) Alemayehu, M. B.; Mitchson, G.; Hanken, B. E.; Asta, M.; Johnson, D. C. *Chem. Mater.* **2014**, *26*, 1859−1866.
(13) Heideman, C.; Tepfer, S.; Lin, Q.; Rostek, R.; Zschack, P.; Anderson, M. D.; Anderson, I. M.; Johnson, D. C. *J. Am. Chem. Soc.* **2013**, *135*, 11055−11062.
(14) Alemayehu, M. B.; Ta, K.; Falmbigl, M.; Johnson, D. C. *Nanoscale* **2015**, DOI: 10.1039/C4NR07338J.
(15) Alemayehu, M. B.; Falmbigl, M.; Ta, K.; Johnscon, D. C. *Chem. Mater.* **2015**, *27*, 2158−2164.
(16) Fister, L.; Johnson, D. C. *J. Am. Chem. Soc.* **1992**, *114*, 4639−4644.
(17) Donovan, J. J.; Tingle, T. N. *Microsc. Soc. Am.* **1996**, *2*, 1−7.

DOI: 10.1021/jacs.5b01556
J. Am. Chem. Soc. 2015, 137, 4831−4839

(18) Alemayehu, M. B.; Falmbigl, M.; Grosse, C.; Ta, K.; Fischer, S. F.; Johnson, D. C. *J. Alloys Compd.* **2015**, *619*, 861−868.
(19) Beekman, M.; Disch, S.; Rouvimov, S.; Kasinathan, D.; Koepernik, K.; Rosner, H.; Zschack, P.; Neumann, W. S. .; Johnson, D. C. *Angew. Chem., Int. Ed. Engl.* **2013**, *52*, 13211−13214.
(20) Chattopadhyay, T.; Pannetier, J.; Von Schnering, H. G. *J. Phys. Chem. Solids* **1986**, *47*, 879−885.
(21) Kadijk, F. *Recl. des Trav. Chim. des Pays-Bas* **1964**, *83*, 768−775.
(22) Kadijk, F. *J. Less Common Met.* **1971**, *23*, 437−441.
(23) Grosse, C.; Atkins, R.; Kirmse, H.; Mogilatenko, A.; Neumann, W.; Johnson, D. C. *J. Alloys Compd.* **2013**, *579*, 507−515.
(24) Py, M.; Haering, R. *Can. J. Phys.* **1983**, *61*, 76−84.
(25) Yoffe, A. D. *Solid State Ionics* **1983**, *10*, 59−70.
(26) Abraham, T.; Juhasz, C.; Silver, J.; Donaldson, J. D.; Road, M. *Solid State Commun.* **1978**, *27*, 1185−1187.

DOI: 10.1021/jacs.5b01556
J. Am. Chem. Soc. 2015, 137, 4831−4839